Proceedings of the ASME 2015 International Design Engineering Technical Conferences & Computers and Information in Engineering Conference
IDETC/CIE 2015
August 2-5, 2015, Boston, Massachusetts, USA

DETC2015-47165

INVESTIGATING MULTISCALE PHENOMENA IN MACHINING: THE EFFECT OF CUTTING-FORCE DISTRIBUTION ALONG THE TOOL'S RAKE FACE ON PROCESS STABILITY

Tamás G. Molnár
Department of Applied Mechanics
Budapest University of Technology and Economics
Budapest, Hungary
e-mail: molnar@mm.bme.hu

Tamás Insperger
Department of Applied Mechanics
Budapest University of Technology and Economics
Budapest, Hungary
e-mail: insperger@mm.bme.hu

S. John Hogan
Department of Engineering Mathematics
University of Bristol
Bristol, UK
e-mail: s.j.hogan@bristol.ac.uk

Gábor Stépán
Department of Applied Mechanics
Budapest University of Technology and Economics
Budapest, Hungary
e-mail: stepan@mm.bme.hu

ABSTRACT

Regenerative machine tool chatter is investigated in a nonlinear single-degree-of-freedom model of turning processes. The nonlinearity arises from the dependence of the cutting-force magnitude on the chip thickness. The cutting-force is modeled as the resultant of a force system distributed along the rake face of the tool. It introduces a distributed delay in the governing equations of the system in addition to the well-known regenerative delay, which is often referred to as the short regenerative effect. The corresponding stability lobe diagrams are depicted, and it is shown that a subcritical Hopf bifurcation occurs along the stability limits in the case of realistic cutting-force distributions. Due to the subcriticality a so-called unsafe zone exists near the stability limits, where the linearly stable cutting process becomes unstable to large perturbations. Based on center-manifold reduction and normal form calculations analytic formulas are obtained to estimate the size of the unsafe zone.

Keywords: metal cutting; turning; delay-differential equation, distributed delay, Hopf bifurcation; bistable zones; limit cycle; subcritical

1 INTRODUCTION

Increasing the accuracy and productivity of metal cutting processes is of key importance in manufacturing technology. One of the most important phenomena that limits the effectiveness of material removal is the occurrence of harmful vibrations during machining, the so-called machine tool chatter. Chatter has many potential negative effects: reduction of the surface quality, limited productivity, enhanced wearing of the tool, noise, and even tool damage. In short, it causes loss of material and energy and increased costs during machining. Therefore, suppressing or avoiding machine tool chatter becomes one of the main goals of manufacturing engineers. The first fundamental works analyzing the dynamics of machining processes and catching the essential phenomena behind chatter are [1, 2]. These works established the theory of regenerative machine tool chatter, namely, they attributed the vibrations to the surface regenerative effect. When the machine tool vibrates relative to the workpiece, the machined surface becomes wavy. In the subsequent cut this wavy surface will alter the chip thickness and the cutting-force, which excites the oscillations in the machine tool-workpiece system. Hence the

surface waviness regenerates during consecutive cuts and vibrations amplify in a self-excited manner. Besides surface regeneration, other effects can also cause vibrations, for example the friction between the tool and the workpiece (frictional chatter) or thermo-mechanical effects during the chip formation (thermo-mechanical chatter, see [3–5]). In this paper we restrict ourselves to the problem of modeling regenerative machine tool chatter.

Since the oscillations of the machine tool-workpiece system depend on the surface formed by the vibrations in the previous cut, delay effects appear in the dynamics of the machining operation. Hence regenerative machine tool chatter is described by delay-differential equations. As discussed in [6], the delay-differential equations possess an infinite-dimensional nature, which makes the dynamics of machining processes very rich and often difficult to analyze. Usually analytic studies are restricted to low-degrees-of-freedom models. The aim of the analysis of the governing delay-differential equations is to create the so-called stability lobe diagrams or stability charts. The stability lobes are the boundary curves of stability in the plane of the spindle speed and the depth of cut separating the chatter-free domains from the regions with machine tool chatter. The parameters of the chatter-free machining process with optimal material removal rate can be selected using the stability lobe diagrams.

In this paper we present stability lobe diagrams of turning operations. According to experimental results (see e.g. [7–9]), there is an upward shift of stability lobes at low spindle speeds. In the past decade several models appeared aiming to explain the enhanced stability of machining at low speeds. Usually the concept of process damping was used, see [7–9], where the increase in stability is believed to appear owing to an additional force, which originates from the interference of the tool flank with the wavy surface of the workpiece. An alternative explanation of the same phenomenon is the so-called short regenerative effect [10]: the interface between the tool and the chip is represented by a finite contact surface, and the cutting-force is modeled as a resultant of a force system distributed along the rake face of the tool. Since the chip needs a certain time to slip along the tool, an additional distributed delay is introduced in the model equations, which is small compared to the regenerative delay. However, this additional small delay is enough to make qualitative changes in the stability lobe diagrams. Thus, the phenomenon of the change in the stability properties for low spindle speeds can be described by a multiscale mechanism, i.e., by the interplay of a large point delay and the short distributed delay. In this paper we extend the model of [10] and consider the short regenerative effect for a model of orthogonal cutting involving the nonlinearity of the cutting-force characteristics, i.e., the nonlinear dependence of the cutting-force on the chip thickness.

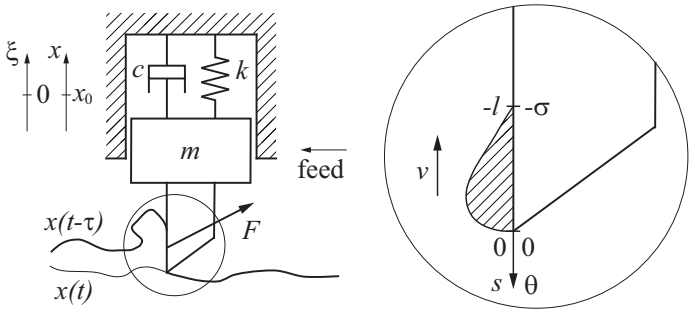

FIGURE 1. SINGLE-DEGREE-OF-FREEDOM MODEL OF TURNING OPERATIONS.

2 MECHANICAL MODEL

In this paper we investigate the single-degree-of-freedom model of orthogonal cutting following [10]. The model is shown in Fig. 1, and it provides a good description of chatter in turning operations if the machining system has a single, well-separated dominant mode. The differential equation governing the relative motion between tool and workpiece becomes

$$m\ddot{x}(t) + c\dot{x}(t) + kx(t) = F_x(t) \,, \tag{1}$$

where m, c and k are the modal mass, damping and stiffness parameters, respectively, and $F_x(t)$ is the x-directional cutting-force component acting on the tool.

2.1 Cutting-force models

Let us model the cutting-force $F_x(t)$ as the resultant of a force system $P_x(t,s)$ distributed along the rake face of the tool. As the contact region between the tool and the workpiece has a finite length l, we use a local coordinate $s \in [-l, 0]$ to describe the cutting-force distribution. We assume that the cutting-force distribution can be decomposed into a magnitude function $F_x^{\mathrm{T}}(t,s)$ and a time-independent weight function $W(s)$. This assumption was verified experimentally for stable stationary cutting using a split-tool [11, 12] and using a sapphire tool [13]. Here we assume that this decomposition is valid in case of small perturbations around the stationary cutting, too. Thus, the expression of the cutting-force reads

$$F_x(t) = \int_{-l}^{0} P_x(t,s)\mathrm{d}s = \int_{-l}^{0} F_x^{\mathrm{T}}(t,s)W(s)\mathrm{d}s \,. \tag{2}$$

The weight function $W(s)$ is normalized in a way that

$$\int_{-l}^{0} W(s)\mathrm{d}s = 1 \,. \tag{3}$$

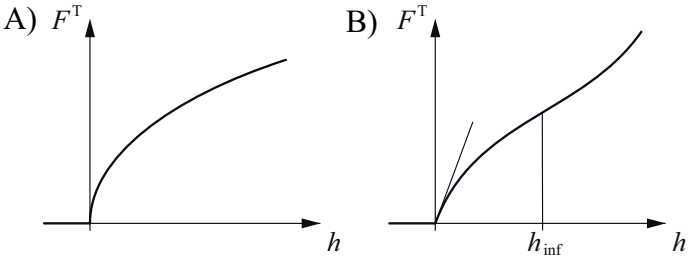

FIGURE 2. FORCE CHARACTERISTICS OF TWO DIFFERENT CUTTING-FORCE MODELS: TAYLOR-FORCE (PANEL A) AND TOBIAS-FORCE (PANEL B).

For the sake of simplicity we assume constant cutting speed v, which can be expressed in terms of the workpiece diameter D and the spindle speed Ω: $v = \Omega D/2$. We suppose that the chip slips along the rake face of the tool with the same constant speed v, and it takes $\sigma = l/v$ time for a certain particle of the chip to travel the length l. Hence we can transform the spatial description of the cutting-force distribution into time using the local temporal coordinate $\theta = s/v$, $\theta \in [-\sigma, 0]$. We rewrite Eqn. (2) in the form

$$F_x(t) = \int_{-\sigma}^{0} F_x^{\mathrm{T}}(t, v\theta) w(\theta) \mathrm{d}\theta \ , \tag{4}$$

where $w(\theta) = vW(v\theta)$ satisfies the criterion

$$\int_{-\sigma}^{0} w(\theta) \mathrm{d}\theta = 1 \ . \tag{5}$$

The magnitude $F_x^{\mathrm{T}}(t, v\theta)$ of the cutting-force distribution depends on the chip thickness $h(t,\theta)$, and there exist various types of force characteristics defining this relation, see e.g. [14] and the references therein. The two most widely used cutting-force magnitude models are the power law introduced in [15] and the cubic force characteristic proposed in [16]. We will refer to these models as the Taylor-force and the Tobias-force, respectively. The Taylor-force can be given in the form

$$F_x^{\mathrm{Taylor}}(t, v\theta) = \begin{cases} K a_{\mathrm{p}} h^q(t,\theta) & \text{if } h(t,\theta) \geq 0 \ , \\ 0 & \text{if } h(t,\theta) < 0 \ , \end{cases} \tag{6}$$

where the cutting coefficient K and the cutting exponent q are constants to be determined by means of experiments, a_{p} is the chip width, and $h(t,\theta)$ is the instantaneous chip thickness along the rake face. We assume $q = 3/4$, which leads to the well-known three-quarter rule. The Tobias-force expression reads

$$F_x^{\mathrm{Tobias}}(t, v\theta) = \begin{cases} a_{\mathrm{p}} \left(\rho_1 h(t,\theta) + \rho_2 h^2(t,\theta) + \rho_3 h^3(t,\theta) \right) & \text{if } h(t,\theta) \geq 0 \ , \\ 0 & \text{if } h(t,\theta) < 0 \ , \end{cases} \tag{7}$$

where the following constants were measured in the experiments reported in [16] for a milling tool of 4 teeth: $\rho_1 = 2.44384 \times 10^{10}$ N/m^2, $\rho_2 = -2.165664 \times 10^{14}$ N/m^3, and $\rho_3 = 8.15076 \times 10^{17}$ N/m^4. The two force characteristics can be observed in Fig. 2. Note that both force models prescribe a monotonously increasing nonlinear cutting-force function. The cutting-force drops to zero for $h(t,\theta) < 0$, which represents the case where the tool loses contact with the workpiece during large-amplitude chatter. In this work however, we assume $h(t,\theta) > 0$ during the entire machining operation. There are two fundamental differences between the two cutting-force models. On the one hand, the Taylor-force has infinitely large derivative (vertical tangent) at zero, which makes the mathematical treatment of the problem difficult near the loss of contact. On the other hand, the cubic force characteristic possesses an inflection point, which has an important role in the dynamics of the nonlinear system (see [17]).

2.2 Instantaneous chip thickness

According to the theory of regenerative machine tool vibrations, the instantaneous chip thickness $h(t,\theta)$ can be given as a function of the actual position of the tool and the position one workpiece revolution ago. Hence we write

$$h(t,\theta) = h_0 + x(t - \tau + \theta) - x(t + \theta) \ , \quad \theta \in [-\sigma, 0] \ , \tag{8}$$

where h_0 is the prescribed (mean) chip thickness, from which the actual chip thickness may differ due to relative vibrations between the tool and the workpiece. Here τ is the regenerative delay, which now equals the rotational period, $\tau = 2\pi/\Omega$. Note that the chip thickness is also a function of θ as it varies along the chip-tool interface.

2.3 Cutting force distribution

The shape $w(\theta)$ of the force distribution is also an important element of the cutting-force model. In the past decades several models were built and measurements were carried out to provide data on the normal and the shear stress distributions along the rake face, see e.g. [11–13, 18–21]. Here, we are interested in the x-directional component of stresses, which, in case of zero rake angle, is the shear stress. Based on the above mentioned articles, two common shapes were suggested for the shear stress distribution. According to [11, 12, 20, 21], the shear stress T has

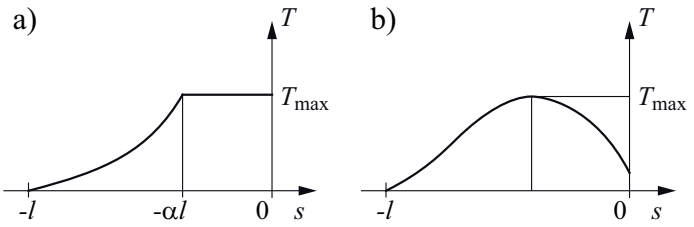

FIGURE 3. DISTRIBUTION OF THE SHEAR STRESS ALONG THE RAKE FACE OF THE TOOL.

a plateau $T_{\max}$ near the tool tip and then decays exponentially to zero at the end of contact (see panel (a) of Fig. 3). Whereas in [13, 19] it was shown that the shear stress T increases from a small value at the tip to a maximum $T_{\max}$, and then decays (see panel (b) of Fig. 3). We will investigate the plateau-and-decay distribution shown in panel (a) of Fig. 3. Two regions can be distinguished in the contact regime: the sticking region (with constant yield shear stress value) and the sliding region (with a decay in the stress). Accordingly, the shape of force distribution can be described by the function

$$w(\theta) = \begin{cases} \dfrac{1}{\sigma}\dfrac{1-\mathrm{e}^{-\alpha+1}}{2-(\alpha+1)\mathrm{e}^{-\alpha+1}} & \text{if } \theta \in [-\alpha\sigma, 0] \ , \\ \dfrac{1}{\sigma}\dfrac{1-\mathrm{e}^{\theta/\sigma+1}}{2-(\alpha+1)\mathrm{e}^{-\alpha+1}} & \text{if } \theta \in [-\sigma, -\alpha\sigma) \ , \end{cases} \tag{9}$$

where $\alpha = l_{\mathrm{s}}/l$ is the ratio of the sticking and the contact length. In [11] measurements gave $\alpha = 0.3..0.4$, whereas in [12] values in the range $\alpha = 0.5..0.6$ were measured. Note that $w(\theta)$ in Eqn. (9) satisfies condition (5).

2.4 Equation of motion

Equation (1) can be written as

$$\ddot{x}(t) + 2\zeta\omega_{\mathrm{n}}\dot{x}(t) + \omega_{\mathrm{n}}^2 x(t) = \frac{1}{m}F_x(t) \ , \tag{10}$$

where $\omega_{\mathrm{n}} = \sqrt{k/m}$ is the natural angular frequency of the undamped system and $\zeta = c/(2\sqrt{km})$ is the damping ratio. Note that $F_x(t)$ is a nonlinear function of x, therefore, Eqn. (10) is a nonlinear differential equation. The ideal chatter-free stationary cutting is associated with the equilibrium

$$x(t) \equiv x_0 = \frac{1}{m\omega_{\mathrm{n}}^2}F_{x0} \ , \tag{11}$$

where $F_{x0} = F_x(t)|_{h(t)\equiv h_0}$. Introduce the new coordinate $\xi(t)$ as

$$\xi(t) = x(t) - x_0 \ . \tag{12}$$

The instantaneous chip thickness expressed in terms of $\xi(t)$ reads

$$h(t,\theta) = h_0 + \xi(t-\tau+\theta) - \xi(t+\theta) \ , \quad \theta \in [-\sigma, 0] \ , \tag{13}$$

while the equation of motion becomes

$$\ddot{\xi}(t) + 2\zeta\omega_{\mathrm{n}}\dot{\xi}(t) + \omega_{\mathrm{n}}^2\xi(t) = \frac{1}{m}\Delta F_x(t) \ . \tag{14}$$

Here $\Delta F_x(t)$ denotes the cutting-force variation and is defined as

$$\Delta F_x(t) = F_x(t) - F_{x0} = \int_{-\sigma}^{0} \Delta F_x^{\mathrm{T}}(t, v\theta) w(\theta) \mathrm{d}\theta \ . \tag{15}$$

The magnitude $\Delta F_x^{\mathrm{T}}(t, v\theta)$ of the cutting-force variation depends on the cutting force model.

In the case of the Taylor-force, we can approximate Eqn. (6) using a Taylor expansion up to third order with respect to $h(t,\theta)$ around h_0. This way Eqns. (6) and (13) give

$$\begin{aligned} \Delta F_x{}^{\mathrm{Taylor}}(t, v\theta) &= K a_{\mathrm{p}} h^q(t,\theta) - K a_{\mathrm{p}} h_0^q \\ &\approx k_1 \left(\xi(t-\tau+\theta) - \xi(t+\theta)\right) + k_2 \left(\xi(t-\tau+\theta) - \xi(t+\theta)\right)^2 \\ &\quad + k_3 \left(\xi(t-\tau+\theta) - \xi(t+\theta)\right)^3 \ , \quad \theta \in [-\sigma, 0] \ , \end{aligned} \tag{16}$$

where the corresponding coefficients are given by

$$k_1 = \frac{3}{4} K a_{\mathrm{p}} h_0^{-1/4} \ , \quad k_2 = -\frac{1}{8h_0}k_1 \ , \quad k_3 = \frac{5}{96h_0^2}k_1 \ . \tag{17}$$

In the case of the Tobias-force, substitution of Eqn. (13) into Eqn. (7) yields the magnitude of the cutting-force variation in the form

$$\begin{aligned} \Delta F_x{}^{\mathrm{Tobias}}(t, v\theta) &= a_{\mathrm{p}} \left(\rho_1 h(t,\theta) + \rho_2 h^2(t,\theta) + \rho_3 h^3(t,\theta)\right) \\ &\quad - a_{\mathrm{p}} \left(\rho_1 h_0 + \rho_2 h_0^2 + \rho_3 h_0^3\right) \\ &= k_1 \left(\xi(t-\tau+\theta) - \xi(t+\theta)\right) + k_2 \left(\xi(t-\tau+\theta) - \xi(t+\theta)\right)^2 \\ &\quad + k_3 \left(\xi(t-\tau+\theta) - \xi(t+\theta)\right)^3 \ , \quad \theta \in [-\sigma, 0] \ , \end{aligned} \tag{18}$$

with the coefficients

$$\begin{aligned} k_1 &= a_{\mathrm{p}} \left(\rho_1 + 2\rho_2 h_0 + 3\rho_3 h_0^2\right) \ , \\ k_2 &= a_{\mathrm{p}} \left(\rho_2 + 3\rho_3 h_0\right) \ , \\ k_3 &= a_{\mathrm{p}} \rho_3 \ . \end{aligned} \tag{19}$$

Consequently, the same cubic polynomial form is obtained for both the Taylor- and the Tobias-force, only the coefficients k_1, k_2 and k_3 are different. Note however, that for the Taylor-force this formalism is only an approximation. The third order expansion is necessary for the subsequent bifurcation analysis. Substitution of Eqns. (15) and (16) or (18) into Eqn. (14) leads to

$$\begin{aligned}\ddot{\xi}(t)+2\zeta\omega_{\mathrm{n}}\dot{\xi}(t)+\omega_{\mathrm{n}}^2\xi(t)\\ =\frac{k_1}{m}\int_{-\sigma}^{0}\Big[(\xi(t-\tau+\theta)-\xi(t+\theta))\\ +\frac{k_2}{k_1}(\xi(t-\tau+\theta)-\xi(t+\theta))^2\\ +\frac{k_3}{k_1}(\xi(t-\tau+\theta)-\xi(t+\theta))^3\Big]w(\theta)\mathrm{d}\theta\ . \quad (20)\end{aligned}$$

Based on Eqn. (20), the tool motion is governed by an autonomous nonlinear differential equation with distributed delay. The kernel $w(\theta)$ of the delay distribution originates from the shape of force distribution along the tool's rake face. The distributed delay is of length σ, and is added to the point delay τ. In this paper we assume that the ratio of the two delays is a given constant ε, i.e., we write

$$\sigma=\varepsilon\tau\ . \quad (21)$$

It is important to note that the ratio ε of the two delays is equivalent to the ratio of the contact length l and the perimeter $D\pi$ of the workpiece (in order to see this, multiply Eqn. (21) by the cutting speed $v=\Omega D/2$, and use the definitions $\sigma=l/v$ and $\tau=2\pi/\Omega$). Therefore, ε can be determined by the stress distribution measurements along the rake face. In the experiments of [11] and [12] the contact length was measured and the corresponding ratio to the workpiece perimeter was around $\varepsilon=0.001..0.01$. Since the point delay τ is called the regenerative delay, we refer to the additional σ-long distributed delay as the *short regenerative delay*, while its influence on the system stability is called the *short regenerative effect*.

We now write Eqn. (20) in dimensionless form. We introduce the dimensionless time $\tilde{t}=\omega_{\mathrm{n}}t$, and replace temporal derivatives by dimensionless ones indicated by prime according to the rule $\dot{\square}=\mathrm{d}\square/\mathrm{d}t=\omega_{\mathrm{n}}\mathrm{d}\square/\mathrm{d}\tilde{t}=\omega_{\mathrm{n}}\square'$. In a similar manner, we also introduce the dimensionless delays $\tilde{\tau}=\omega_{\mathrm{n}}\tau$ and $\tilde{\sigma}=\omega_{\mathrm{n}}\sigma$, as well as the dimensionless local temporal coordinate $\tilde{\theta}=\omega_{\mathrm{n}}\theta$, $\tilde{\theta}\in[-\tilde{\sigma},0]$. We can also rescale $w(\theta)$ as $\tilde{w}(\tilde{\theta})=w(\omega_{\mathrm{n}}\theta)/\omega_{\mathrm{n}}$ and $\xi(t)$ as $\tilde{\xi}(t)=\xi(t)/h_0$. After dropping the tilde

$$\begin{aligned}\xi''(t)+2\zeta\xi'(t)+\xi(t)\\ =p\int_{-\sigma}^{0}\Big[(\xi(t-\tau+\theta)-\xi(t+\theta))\\ +\eta_2(\xi(t-\tau+\theta)-\xi(t+\theta))^2\\ +\eta_3(\xi(t-\tau+\theta)-\xi(t+\theta))^3\Big]w(\theta)\mathrm{d}\theta\ , \quad (22)\end{aligned}$$

where $p=k_1/(m\omega_{\mathrm{n}}^2)$ is the dimensionless chip width being proportional to the actual chip width a_{p}. The dimensionless cutting-force coefficients η_2 and η_3 can be expressed in the form

$$\eta_2=\frac{k_2}{k_1}h_0=\begin{cases}-\dfrac{1}{8} & \text{for Taylor-force ,}\\ \dfrac{\rho_2+3\rho_3h_0}{\rho_1+2\rho_2h_0+3\rho_3h_0^2}h_0 & \text{for Tobias-force ,}\end{cases} \quad (23)$$

$$\eta_3=\frac{k_3}{k_1}h_0^2=\begin{cases}\dfrac{5}{96} & \text{for Taylor-force ,}\\ \dfrac{\rho_3}{\rho_1+2\rho_2h_0+3\rho_3h_0^2}h_0^2 & \text{for Tobias-force .}\end{cases} \quad (24)$$

Note that the coefficients η_2 and η_3 are functions of the mean chip thickness h_0 only in the case of the Tobias-force, they are constant for the Taylor-force. The subsequent sections discuss the stability and bifurcation analysis of Eqn. (22).

LINEAR STABILITY ANALYSIS

First we discuss the linear stability analysis of Eqn. (22). Linearizing the governing equation around the trivial equilibrium $\xi(t)\equiv 0$ yields

$$\begin{aligned}\xi''(t)+2\zeta\xi'(t)+\xi(t)\\ =p\int_{-\sigma}^{0}[\xi(t-\tau+\theta)-\xi(t+\theta)]w(\theta)\mathrm{d}\theta\ . \quad (25)\end{aligned}$$

The stability analysis of Eqn. (25) has already been carried out in [10]. At the stability boundaries a Hopf bifurcation occurs, which gives rise to oscillations at a well-defined dimensionless angular frequency ω. Note that a fold bifurcation cannot happen in this system. In [10] the D-subdivision method was used to compute the linear stability limits, which are parameterized by

$\psi = \omega\tau$ and assume the form

$$\begin{aligned}
\omega(\psi) &= -\zeta\frac{R_0(\psi)}{S_0(\psi)} + \sqrt{\zeta^2\frac{R_0^2(\psi)}{S_0^2(\psi)}+1}\,, \\
p_{\mathrm{st}}(\psi) &= -\frac{2\zeta\omega(\psi)}{S_0(\psi)}\,, \\
\Omega(\psi) &= \frac{2\pi}{\tau(\psi)} = \frac{2\pi\omega(\psi)}{\psi}\,,
\end{aligned} \tag{26}$$

where $R_0(\psi)$ and $S_0(\psi)$ are the following integral terms:

$$\begin{aligned}
R_0(\psi) &= \int_{-\sigma}^{0}\left[\cos(\omega\theta)-\cos(\omega(\theta-\tau))\right]w(\theta)\mathrm{d}\theta = \frac{\omega^2(\psi)-1}{p_{\mathrm{st}}(\psi)}, \\
S_0(\psi) &= \int_{-\sigma}^{0}\left[\sin(\omega\theta)-\sin(\omega(\theta-\tau))\right]w(\theta)\mathrm{d}\theta = -\frac{2\zeta\omega(\psi)}{p_{\mathrm{st}}(\psi)}\,.
\end{aligned} \tag{27}$$

Throughout the bifurcation analysis of the next section, we will use the dimensionless chip width p as a bifurcation parameter. Therefore, in order to distinguish between the actual value of the bifurcation parameter and its value at the linear stability boundary, we denoted the latter one by $p_{\mathrm{st}}(\psi)$ in Eqn. (26).

It is also important to highlight that the parameter ψ has a physical meaning, namely, it represents the phase shift between the waves on the machined surface cut momentarily and one revolution ago. The D-curves in Eqn. (26) can be depicted on the plane of the dimensionless angular velocity Ω and dimensionless chip width p, resulting in the so-called stability lobe diagrams or stability charts. As for $\Omega = 0$ and for $p = 0$ no cutting is performed, these lines are always part of the stable region. The linear stability charts will be presented later in Fig. 4 together with the global stability boundaries.

From this point on we investigate the Hopf bifurcation, i.e., we consider the system at the stability limits (26). For the sake of simplicity, we omit the argument ψ. The bifurcation parameter is chosen to be the dimensionless chip width p.

First let us prove that there is indeed a Hopf bifurcation at the stability boundaries. In order to do so we analyze the eigenvalues (or characteristic exponents) of Eqn. (25), which are the roots of the characteristic function

$$D(\lambda) = \lambda^2 + 2\zeta\lambda + 1 + p\int_{-\sigma}^{0}\left[\mathrm{e}^{\lambda\theta} - \mathrm{e}^{\lambda(\theta-\tau)}\right]w(\theta)\mathrm{d}\theta\,. \tag{28}$$

The system is asymptotically stable provided that all infinitely many eigenvalues lie in the negative half of the complex plane. At the Hopf stability limits two eigenvalues lie on the imaginary axis and the other infinitely many have negative real parts. However, according to [22, 23] it is necessary for a Hopf bifurcation to occur that the critical eigenvalues of the system not just touch the imaginary axis but cross it with positive speed as the bifurcation parameter p is increased. Hence the real part of the critical characteristic exponents $\lambda = \pm\mathrm{i}\omega$ must increase with p, i.e., the following derivative must be positive

$$\gamma = \Re\left(\left.\frac{\mathrm{d}\lambda}{\mathrm{d}p}\right|_{\lambda=\mathrm{i}\omega}\right) = \Re\left(\left.-\frac{\dfrac{\partial D}{\partial p}}{\dfrac{\partial D}{\partial\lambda}}\right|_{\lambda=\mathrm{i}\omega}\right) = -\frac{R_0q_1+S_0q_2}{q_1^2+q_2^2}\,, \tag{29}$$

where

$$\begin{aligned}
q_1 &= p_{\mathrm{st}}R_1 + 2\zeta\,, \\
q_2 &= p_{\mathrm{st}}S_1 + 2\omega\,,
\end{aligned} \tag{30}$$

with

$$\begin{aligned}
R_1 &= \frac{\psi}{\omega}\frac{\mathrm{d}S_0}{\mathrm{d}\psi}\,, \\
S_1 &= -\frac{\psi}{\omega}\frac{\mathrm{d}R_0}{\mathrm{d}\psi}\,.
\end{aligned} \tag{31}$$

Equations (30) and (31) are obtained by expressing the derivative $\mathrm{d}\lambda/\mathrm{d}p$ from the characteristic equation $D(\lambda) = 0$ by implicit differentiation. The crossing speed γ is positive if its numerator γ_{N} is also positive. It can be shown that γ_{N} can be equivalently be written in the form

$$\gamma_{\mathrm{N}} = -R_0q_1 - S_0q_2 = -\frac{2\zeta}{p_{\mathrm{st}}}(\omega^2+1)\omega\frac{2\pi}{\Omega^2}\frac{\mathrm{d}\Omega}{\mathrm{d}\psi}\,. \tag{32}$$

Consequently, the condition for the existence of a Hopf bifurcation becomes

$$\gamma > 0 \Leftrightarrow \mathrm{d}\Omega/\mathrm{d}\psi < 0 \Leftrightarrow \mathrm{d}\tau/\mathrm{d}\psi > 0\,. \tag{33}$$

Based on the physics of the problem, we can propose an argument why the above inequality holds. If we increase the spindle speed of the workpiece, the waves on the machined surface become more dense with smaller phase shift, hence $\mathrm{d}\psi/\mathrm{d}\Omega < 0$. Furthermore, it also seems reasonable that the phase shift of a physical system increases as the system delay increases, that is, $\mathrm{d}\tau/\mathrm{d}\psi > 0$ holds. These conditions are equivalent to inequality (33). However, as no strict mathematical proof is given, the condition $\gamma > 0$ was checked numerically by plotting the $\gamma(\psi)$ function for each case study in this article.

Therefore, we can conclude that Hopf bifurcation occurs at the stability limits, which results in the emergence of a periodic

orbit in the vicinity of the equilibrium of the nonlinear system. In the following section we reduce the critical infinite-dimensional system to a finite dimensional center manifold and carry out normal form calculations in order to determine the stability and amplitude of the periodic orbits.

CENTER MANIFOLD REDUCTION

The subsequent analysis is based on the theory of functional differential equations summarized in [24] and follows the steps of [17, 25], where the orthogonal cutting model was considered with a concentrated cutting-force. Note that the concentrated cutting-force model is the special case of the distributed one with a Dirac delta kernel function $w(\theta) = \delta(\theta)$. As a first step of the analysis, Eqn. (22) is written in first-order form

$$\mathbf{y}'(t) = \mathbf{L}\mathbf{y}(t) + \mathbf{R}\int_{-\sigma}^{0} \left[\mathbf{y}(t-\tau+\theta) - \mathbf{y}(t+\theta)\right] w(\theta)\mathrm{d}\theta + \mathbf{g}(\mathbf{y}_t) \,, \tag{34}$$

where $\mathbf{y}(t)$ is the vector of state variables, $\mathbf{L}$ is the linear, $\mathbf{R}$ is the retarded coefficient matrix, and $\mathbf{g}(\mathbf{y}_t)$ contains all nonlinear terms. These quantities are defined as

$$\mathbf{y}(t) = \begin{bmatrix} \xi(t) \\ \xi'(t) \end{bmatrix}, \; \mathbf{L} = \begin{bmatrix} 0 & 1 \\ -1 & -2\zeta \end{bmatrix}, \; \mathbf{R} = \begin{bmatrix} 0 & 0 \\ p & 0 \end{bmatrix}, \; \mathbf{g}(\mathbf{y}_t) = \begin{bmatrix} 0 \\ g_2(\mathbf{y}_t) \end{bmatrix},$$
$$g_2(\mathbf{y}_t) = p\int_{-\sigma}^{0} \Big[\eta_2 \left(y_1(t-\tau+\theta) - y_1(t+\theta)\right)^2 + \eta_3 \left(y_1(t-\tau+\theta) - y_1(t+\theta)\right)^3\Big] w(\theta)\mathrm{d}\theta \,, \tag{35}$$

while $\mathbf{y}_t$ is introduced below. Since delay-differential equations exhibit an infinite dimensional nature, it is advantageous to use a state function instead of a vector of state variables to describe the system. Following [6, 24] we define the shift

$$\mathbf{y}_t(\vartheta) = \mathbf{y}(t+\vartheta) \,, \quad \vartheta \in [-\sigma-\tau, 0] \,, \tag{36}$$

where $\mathbf{y}_t : [-\sigma-\tau, 0] \to \mathbb{R}^2 \in \mathscr{H}$. In other words, the state of the system along the whole time interval $[t-\sigma-\tau, t]$ is represented by the function $\mathbf{y}_t$ defined in the Hilbert space $\mathscr{H}$ of continuously differentiable vector valued functions. Accordingly, we characterize the evolution of the system in the Hilbert space $\mathscr{H}$ by formulating the operator differential equation corresponding to Eqn. (34)

$$\mathbf{y}_t'(\vartheta) = \mathscr{A}\mathbf{y}_t + \mathscr{F}(\mathbf{y}_t) \,, \tag{37}$$

where $\mathscr{A}, \mathscr{F} : \mathscr{H} \to \mathscr{H}$ are the linear and the nonlinear operators, respectively. The linear operator is defined as

$$\mathscr{A}\mathbf{u} = \begin{cases} \mathbf{u}^{\mathrm{o}}(\vartheta) & \text{if } \vartheta \in [-\sigma-\tau, 0) \,, \\ \mathbf{L}\mathbf{u}(0) + \mathbf{R}\displaystyle\int_{-\sigma}^{0} \left[\mathbf{u}(\theta-\tau) - \mathbf{u}(\theta)\right] w(\theta)\mathrm{d}\theta & \text{if } \vartheta = 0 \,, \end{cases} \tag{38}$$

where the notation $\square^{\mathrm{o}} = \mathrm{d}\square/\mathrm{d}\vartheta$ is used for the derivative with respect to ϑ. The definition of the nonlinear operator is

$$\mathscr{F}(\mathbf{u}) = \begin{cases} \mathbf{0} & \text{if } \vartheta \in [-\sigma-\tau, 0) \,, \\ \mathbf{g}(\mathbf{u}) & \text{if } \vartheta = 0 \,. \end{cases} \tag{39}$$

The main idea behind the center manifold reduction is discussed in [24]. In this work a decomposition of $\mathscr{H}$ is proposed, which is the extension of the Jordan canonical form of ordinary differential equations to infinite dimensional systems. The decomposition is based on the eigenvalues of the corresponding linear system, and it allows us to separate the stable, unstable and center subspaces. In order to study the system that undergoes a Hopf bifurcation at the stability limit, we can decompose the infinite-dimensional space with respect to the critical eigenvalues $\lambda = \pm\mathrm{i}\omega$. As all the other eigenvalues have negative real parts, we get a two-dimensional critical subspace which attracts exponentially all the solutions of the differential equation. The two-dimensional attractive subsystem embedded in the infinite-dimensional phase space is called the center manifold. Therefore, if we are interested only in the long-term dynamics of the system, we can analyze the flow on the center manifold and study a two-dimensional ordinary differential equation instead of an infinite-dimensional delayed system.

Since the center manifold is tangent to the plane spanned by the real and imaginary parts of the critical eigenfunctions (infinite-dimensional eigenvectors) of $\mathscr{A}$, we first calculate these eigenvectors, and later we continue with the decomposition theorem of [24]. The critical eigenvectors $\mathbf{s}_{1,2}(\vartheta)$ are defined by

$$\mathscr{A}\mathbf{s}_{1,2}(\vartheta) = \pm\mathrm{i}\omega\mathbf{s}_{1,2}(\vartheta) \,. \tag{40}$$

Since the eigenvectors are complex conjugate pairs, we write them in the form $\mathbf{s}_{1,2}(\vartheta) = \mathbf{s}_{\mathrm{R}}(\vartheta) \pm \mathrm{i}\mathbf{s}_{\mathrm{I}}(\vartheta)$. Decomposition of the eigenvector equation into real and imaginary parts yields

$$\mathscr{A}\mathbf{s}(\vartheta) = \mathbf{B}_{4\times4}\mathbf{s}(\vartheta) \,, \tag{41}$$

provided that $\mathbf{s}(\vartheta) = [\mathbf{s}_{\mathrm{R}}(\vartheta)\ \mathbf{s}_{\mathrm{I}}(\vartheta)]^{\mathrm{T}}$ and

$$\mathbf{B}_{4\times4} = \begin{bmatrix} \mathbf{0} & -\omega\mathbf{I} \\ \omega\mathbf{I} & \mathbf{0} \end{bmatrix}, \tag{42}$$

where $\mathbf{I}$ and $\mathbf{0}$ are the 2×2 identity and zero matrices, respectively. According to the definition of $\mathscr{A}$, Eqn. (41) implies a boundary value problem. For $\vartheta\in[-\sigma-\tau,0)$ we get the differential equation

$$\mathbf{s}^{\mathrm{o}}(\vartheta)=\mathbf{B}_{4\times4}\mathbf{s}(\vartheta)\ . \tag{43}$$

The solution can be given in the form

$$\mathbf{s}(\vartheta)=\mathrm{e}^{\mathbf{B}_{4\times4}\vartheta}\mathbf{c}\ , \tag{44}$$

where $\mathbf{c}=[\mathbf{c}_1\ \mathbf{c}_2]^{\mathrm{T}}=[c_{11}\ c_{12}\ c_{21}\ c_{22}]^{\mathrm{T}}$ is a constant determined by the boundary conditions, and the matrix exponential of $\mathbf{B}$ can be given in the form

$$\mathrm{e}^{\mathbf{B}_{4\times4}\vartheta}=\begin{bmatrix}\cos(\omega\vartheta)\mathbf{I} & -\sin(\omega\vartheta)\mathbf{I}\\ \sin(\omega\vartheta)\mathbf{I} & \cos(\omega\vartheta)\mathbf{I}\end{bmatrix}\ . \tag{45}$$

Eqn. (41) provides the following boundary conditions for $\vartheta=0$:

$$\mathbf{L}_{4\times4}\mathbf{s}(0)+\mathbf{R}_{4\times4}\int_{-\sigma}^{0}\left[\mathbf{s}(\theta-\tau)-\mathbf{s}(\theta)\right]w(\theta)\mathrm{d}\theta=\mathbf{B}_{4\times4}\mathbf{s}(0)\ , \tag{46}$$

where

$$\mathbf{L}_{4\times4}=\begin{bmatrix}\mathbf{L} & \mathbf{0}\\ \mathbf{0} & \mathbf{L}\end{bmatrix},\quad \mathbf{R}_{4\times4}=\begin{bmatrix}\mathbf{R} & \mathbf{0}\\ \mathbf{0} & \mathbf{R}\end{bmatrix}\ . \tag{47}$$

Substituting the trial solution (44) into the boundary condition (46) gives the value of $\mathbf{c}$. We can choose two components arbitrarily, therefore we write $c_{11}=1$ and $c_{21}=0$, by which we obtain $\mathbf{c}=[\mathbf{c}_1\ \mathbf{c}_2]^{\mathrm{T}}=[1\ 0\ 0\ \omega]^{\mathrm{T}}$ and

$$\mathbf{s}_{\mathrm{R}}(\vartheta)=\begin{bmatrix}\cos(\omega\vartheta)\\ -\omega\sin(\omega\vartheta)\end{bmatrix},\quad \mathbf{s}_{\mathrm{I}}(\vartheta)=\begin{bmatrix}\sin(\omega\vartheta)\\ \omega\cos(\omega\vartheta)\end{bmatrix}\ . \tag{48}$$

The decomposition theorem of [24] also uses the so-called left-hand side eigenvectors which are the eigenvectors of the operator $\mathscr{A}^{\mathrm{H}}$ being formally adjoint to $\mathscr{A}$ relative to a certain bilinear form. The formal adjoint $\mathscr{A}^{\mathrm{H}}$ must satisfy

$$(\mathbf{v},\mathscr{A}\mathbf{u})=(\mathscr{A}^{\mathrm{H}}\mathbf{v},\mathbf{u})\ . \tag{49}$$

where $\mathbf{u}:[-\sigma-\tau,0]\to\mathbb{R}^2\in\mathscr{H}$ and $\mathbf{v}:[0,\sigma+\tau]\to\mathbb{R}^2\in\mathscr{H}^{\mathrm{H}}$, i.e., it is the element of the adjoint space. The operation $(\ ,\ ):\mathscr{H}^{\mathrm{H}}\times\mathscr{H}\to\mathbb{R}$ indicates the bilinear form. The definition of the formal adjoint can be found in [24] and here it takes the form

$$\mathscr{A}^{\mathrm{H}}\mathbf{v}=\begin{cases}-\mathbf{v}^{\mathrm{o}}(\vartheta) & \text{if } \vartheta\in(0,\sigma+\tau]\ ,\\ \mathbf{L}^{\mathrm{H}}\mathbf{v}(0)+\mathbf{R}^{\mathrm{H}}\displaystyle\int_{-\sigma}^{0}\left[\mathbf{v}(\tau-\theta)-\mathbf{v}(-\theta)\right]w(\theta)\mathrm{d}\theta & \\ & \text{if } \vartheta=0\ .\end{cases} \tag{50}$$

whereas the bilinear form also defined in [24] now becomes

$$\begin{aligned}(\mathbf{u},\mathbf{v})=&\mathbf{u}^{\mathrm{H}}(0)\mathbf{v}(0)+\int_{-\sigma}^{0}\int_{-\theta}^{0}\mathbf{u}^{\mathrm{H}}(\vartheta)\left(\mathbf{R}w(\theta)\right)\mathbf{v}(\vartheta+\theta)\mathrm{d}\vartheta\mathrm{d}\theta\\ &-\int_{-\sigma-\tau}^{-\tau}\int_{-\theta}^{0}\mathbf{u}^{\mathrm{H}}(\vartheta)\left(\mathbf{R}w(\tau+\theta)\right)\mathbf{v}(\vartheta+\theta)\mathrm{d}\vartheta\mathrm{d}\theta\ .\end{aligned} \tag{51}$$

In order to calculate the left-hand side eigenvectors $\mathbf{n}_{1,2}(\varphi)$, we repeat the same eigenvector computation procedure for $\mathscr{A}^{\mathrm{H}}$ as for $\mathscr{A}$. Since the eigenvalues of $\mathscr{A}^{\mathrm{H}}$ are the complex conjugates to those of $\mathscr{A}$, we write

$$\mathscr{A}^{\mathrm{H}}\mathbf{n}_{1,2}(\varphi)=\mp\mathrm{i}\omega\mathbf{n}_{1,2}(\varphi)\ . \tag{52}$$

A decomposition into real and imaginary parts yields

$$\mathscr{A}^{\mathrm{H}}\mathbf{n}(\varphi)=\mathbf{B}_{4\times4}^{\mathrm{H}}\mathbf{n}(\varphi)\ , \tag{53}$$

where the superscript H indicates conjugate transpose and $\mathbf{n}_{1,2}(\varphi)=\mathbf{n}_{\mathrm{R}}(\varphi)\pm\mathrm{i}\mathbf{n}_{\mathrm{I}}(\varphi)$. Hence a similar boundary value problem is obtained as in Eqn. (41). The only difference is that we cannot choose the coefficients of $\mathbf{n}(\varphi)$ arbitrarily as we did for $\mathbf{s}(\vartheta)$ by writing $c_{11}=1$ and $c_{21}=0$. In order to apply the decomposition theorem of [24], $\mathbf{n}(\varphi)$ must satisfy the orthonormality condition

$$\begin{aligned}(\mathbf{n}_{\mathrm{R}},\mathbf{s}_{\mathrm{R}})=&1\ ,\\ (\mathbf{n}_{\mathrm{R}},\mathbf{s}_{\mathrm{I}})=&0\ .\end{aligned} \tag{54}$$

We get the final result for the left-hand side eigenfunctions in the form

$$\begin{aligned}\mathbf{n}_{\mathrm{R}}(\varphi)=&\frac{2}{q_1^2+q_2^2}\begin{bmatrix}(2\zeta q_1+\omega q_2)\cos(\omega\varphi)+(\omega q_1-2\zeta q_2)\sin(\omega\varphi)\\ q_1\cos(\omega\varphi)-q_2\sin(\omega\varphi)\end{bmatrix},\\ \mathbf{n}_{\mathrm{I}}(\varphi)=&\frac{2}{q_1^2+q_2^2}\begin{bmatrix}(-\omega q_1+2\zeta q_2)\cos(\omega\varphi)+(2\zeta q_1+\omega q_2)\sin(\omega\varphi)\\ q_2\cos(\omega\varphi)+q_1\sin(\omega\varphi)\end{bmatrix}.\end{aligned} \tag{55}$$

According to [24], we can decompose the solution space as

$$\mathbf{y}_t(\vartheta) = z_1(t)\mathbf{s}_{\mathrm{R}}(\vartheta) + z_2(t)\mathbf{s}_{\mathrm{I}}(\vartheta) + \mathbf{y}_{tn}(t)(\vartheta) \,, \tag{56}$$

where $z_1(t)$ and $z_2(t)$ describe the behavior of the critical subsystem as they are local coordinates on the center manifold, whereas $\mathbf{y}_{tn}(t)$ accounts for the remaining infinite-dimensional subsystem with coordinates perpendicular to the center manifold. The decomposition theorem gives the formula of the different components:

$$\begin{aligned} z_1(t) =& (\mathbf{n}_{\mathrm{R}}, \mathbf{y}_t) \,, \\ z_2(t) =& (\mathbf{n}_{\mathrm{I}}, \mathbf{y}_t) \,, \\ \mathbf{y}_{tn}(t)(\vartheta) =& \mathbf{y}_t(\vartheta) - z_1(t)\mathbf{s}_{\mathrm{R}}(\vartheta) - z_2(t)\mathbf{s}_{\mathrm{I}}(\vartheta) \,. \end{aligned} \tag{57}$$

Differentiating these relations with respect to time and using Eqns. (37), (56) and (40), the following differential equation can be obtained

$$\begin{aligned} \begin{bmatrix} z_1' \\ z_2' \\ \mathbf{y}_{tn}' \end{bmatrix} =& \begin{bmatrix} 0 & \omega & \mathscr{O} \\ -\omega & 0 & \mathscr{O} \\ \mathfrak{o} & \mathfrak{o} & \mathscr{A} \end{bmatrix} \begin{bmatrix} z_1 \\ z_2 \\ \mathbf{y}_{tn} \end{bmatrix} \\ &+ \begin{bmatrix} n_{\mathrm{R}2}(0)\mathscr{F}_2(0) \\ n_{\mathrm{I}2}(0)\mathscr{F}_2(0) \\ -n_{\mathrm{R}2}(0)\mathscr{F}_2(0)\mathbf{s}_{\mathrm{R}} - n_{\mathrm{I}2}(0)\mathscr{F}_2(0)\mathbf{s}_{\mathrm{I}} + \mathscr{F} \end{bmatrix}, \end{aligned} \tag{58}$$

where $\mathfrak{o} : \mathbb{R} \to \mathscr{H}$ and $\mathscr{O} : \mathscr{H} \to \mathbb{R}$ are zero operators, and subscript 2 indicates the second component of vectors. Although the two-dimensional critical subspace is now linearly decoupled, there is still a coupling through the nonlinear term $\mathscr{F}_2(0)$. In order to obtain a decoupled system up to the third order (i.e., to get a third-order normal form), $\mathscr{F}_2(0)$ should be expressed in terms of z_1 and z_2 up to third order. For this transformation, we need at least a second-order approximation for the center manifold itself:

$$\mathbf{y}_{tn}(\vartheta) = \frac{1}{2}\left[\mathbf{h}_1(\vartheta)z_1^2 + 2\mathbf{h}_2(\vartheta)z_1z_2 + \mathbf{h}_3(\vartheta)z_2^2\right] \,. \tag{59}$$

The coefficients $\mathbf{h}_1(\vartheta)$, $\mathbf{h}_2(\vartheta)$ and $\mathbf{h}_3(\vartheta)$ can be calculated as follows. First we differentiate Eqn. (59) with respect to time and substitute the different rows of Eqn. (56) to express temporal derivatives. Then the case $\vartheta \in [-\sigma - \tau, 0)$ is considered, and the definitions of $\mathscr{A}$ and $\mathscr{F}$ are substituted from Eqns. (38)-(39). We also substitute the derivative of Eqn. (59) with respect to ϑ, and use a second-order approximation for $\mathscr{F}_2(0)$ as

$$\begin{aligned} \mathscr{F}_2(0) \approx& \frac{1}{2}\left.\frac{\partial^2\mathscr{F}_2(0)}{\partial z_1^2}\right|_0 z_1^2 + \left.\frac{\partial^2\mathscr{F}_2(0)}{\partial z_1\partial z_2}\right|_0 z_1z_2 + \frac{1}{2}\left.\frac{\partial^2\mathscr{F}_2(0)}{\partial z_2^2}\right|_0 z_2^2 \\ =& F_1z_1^2 + F_2z_1z_2 + F_3z_2^2 \,, \end{aligned} \tag{60}$$

where the subscript 0 indicates the point $z_1 = 0$, $z_2 = 0$ and $y_{tn1} = 0$. Finally, we consider a polynomial balance, and collect the coefficients of the second order terms of z_1 and z_2. This way we end up with the differential equation

$$\mathbf{h}^{\mathrm{o}}(\vartheta) = \mathbf{C}_{6\times6}\mathbf{h}(\vartheta) + \mathbf{p}\cos(\omega\vartheta) + \mathbf{q}\sin(\omega\vartheta) \,, \tag{61}$$

where

$$\begin{aligned} \mathbf{h}(\vartheta) =& \begin{bmatrix} \mathbf{h}_1(\vartheta) \\ \mathbf{h}_2(\vartheta) \\ \mathbf{h}_3(\vartheta) \end{bmatrix}, \quad \mathbf{C}_{6\times6} = \begin{bmatrix} \mathbf{0} & -2\omega\mathbf{I} & \mathbf{0} \\ \omega\mathbf{I} & \mathbf{0} & -\omega\mathbf{I} \\ \mathbf{0} & 2\omega\mathbf{I} & \mathbf{0} \end{bmatrix}, \\ \mathbf{p} =& \begin{bmatrix} 2n_{\mathrm{R}2}(0)F_1\mathbf{c}_1 + 2n_{\mathrm{I}2}(0)F_1\mathbf{c}_2 \\ n_{\mathrm{R}2}(0)F_2\mathbf{c}_1 + n_{\mathrm{I}2}(0)F_2\mathbf{c}_2 \\ 2n_{\mathrm{R}2}(0)F_3\mathbf{c}_1 + 2n_{\mathrm{I}2}(0)F_3\mathbf{c}_2 \end{bmatrix}, \\ \mathbf{q} =& \begin{bmatrix} -2n_{\mathrm{R}2}(0)F_1\mathbf{c}_2 + 2n_{\mathrm{I}2}(0)F_1\mathbf{c}_1 \\ -n_{\mathrm{R}2}(0)F_2\mathbf{c}_2 + n_{\mathrm{I}2}(0)F_2\mathbf{c}_1 \\ -2n_{\mathrm{R}2}(0)F_3\mathbf{c}_2 + 2n_{\mathrm{I}2}(0)F_3\mathbf{c}_1 \end{bmatrix} . \end{aligned} \tag{62}$$

The solution of Eqn. (61) reads

$$\mathbf{h}(\vartheta) = \mathbf{M}\cos(\omega\vartheta) + \mathbf{N}\sin(\omega\vartheta) + \mathrm{e}^{\mathbf{C}_{6\times6}\vartheta}\mathbf{K} \,, \tag{63}$$

where the matrix exponential can be written in the form

$$\mathrm{e}^{\mathbf{C}_{6\times6}\vartheta} = \begin{bmatrix} \frac{1+\cos(2\omega\vartheta)}{2}\mathbf{I} & -\sin(2\omega\vartheta)\mathbf{I} & \frac{1-\cos(2\omega\vartheta)}{2}\mathbf{I} \\ \frac{\sin(2\omega\vartheta)}{2}\mathbf{I} & \cos(2\omega\vartheta)\mathbf{I} & -\frac{\sin(2\omega\vartheta)}{2}\mathbf{I} \\ \frac{1-\cos(2\omega\vartheta)}{2}\mathbf{I} & \sin(2\omega\vartheta)\mathbf{I} & \frac{1+\cos(2\omega\vartheta)}{2}\mathbf{I} \end{bmatrix} . \tag{64}$$

Substituting the trial solution (63) back into the differential equation (61) and considering a harmonic balance allows us to calculate the coefficients $\mathbf{M}$ and $\mathbf{N}$ in the form

$$\begin{bmatrix} \mathbf{M} \\ \mathbf{N} \end{bmatrix} = \begin{bmatrix} -\mathbf{C}_{6\times6} & \omega\mathbf{I}_{6\times6} \\ -\omega\mathbf{I}_{6\times6} & -\mathbf{C}_{6\times6} \end{bmatrix}^{-1} \begin{bmatrix} \mathbf{p} \\ \mathbf{q} \end{bmatrix} . \tag{65}$$

In order to calculate $\mathbf{K}$ we need a boundary condition corresponding to Eqn. (61). Therefore, we return to Eqn. (59), we again differentiate it with respect to time, and substitute the three rows of Eqn. (56) as before. This time however, we consider $\theta = 0$, and substitute the definitions (38)-(39) of $\mathscr{A}$ and $\mathscr{F}$ accordingly. Using the second-order approximation (60), a harmonic balance on the second-order terms of z_1 and z_2 yields the boundary condition

$$\mathbf{P}_{6\times6}\mathbf{h}(0) + \mathbf{R}_{6\times6}\int_{-\sigma}^{0}\left[\mathbf{h}(\theta-\tau) - \mathbf{h}(\theta)\right]w(\theta)\mathrm{d}\theta = \mathbf{p} + \mathbf{r} \,, \tag{66}$$

where

$$\mathbf{R}_{6\times6}=\begin{bmatrix}\mathbf{R}&\mathbf{0}&\mathbf{0}\\ \mathbf{0}&\mathbf{R}&\mathbf{0}\\ \mathbf{0}&\mathbf{0}&\mathbf{R}\end{bmatrix},\quad \mathbf{L}_{6\times6}=\begin{bmatrix}\mathbf{L}&\mathbf{0}&\mathbf{0}\\ \mathbf{0}&\mathbf{L}&\mathbf{0}\\ \mathbf{0}&\mathbf{0}&\mathbf{L}\end{bmatrix},$$

$$\mathbf{P}_{6\times6}=\begin{bmatrix}\mathbf{L}&2\omega\mathbf{I}&\mathbf{0}\\ -\omega\mathbf{I}&\mathbf{L}&\omega\mathbf{I}\\ \mathbf{0}&-2\omega\mathbf{I}&\mathbf{L}\end{bmatrix}=\mathbf{L}_{6\times6}-\mathbf{C}_{6\times6},\quad \mathbf{r}=\begin{bmatrix}0\\ -2F_1\\ 0\\ -F_2\\ 0\\ -2F_3\end{bmatrix}. \tag{67}$$

After substituting the trial solution (63) into the boundary condition (66) we can express $\mathbf{K}$ in the form

$$\mathbf{K}=(\mathbf{P}_{6\times6}+\mathbf{R}_{6\times6}\mathbf{Q}_{6\times6})^{-1}\times \\ (\mathbf{p}+\mathbf{r}-\mathbf{P}_{6\times6}\mathbf{M}+\mathbf{R}_{6\times6}\mathbf{M}R_0(\psi)+\mathbf{R}_{6\times6}\mathbf{N}S_0(\psi)), \tag{68}$$

where

$$\mathbf{Q}_{6\times6}=\int_{-\sigma}^{0}\left(\mathrm{e}^{\mathbf{C}_{6\times6}(\theta-\tau)}-\mathrm{e}^{\mathbf{C}_{6\times6}\theta}\right)w(\theta)\mathrm{d}\theta \\ =\begin{bmatrix}-\frac{R_0(2\psi)}{2}\mathbf{I}&S_0(2\psi)\mathbf{I}&\frac{R_0(2\psi)}{2}\\ -\frac{S_0(2\psi)}{2}\mathbf{I}&-R_0(2\psi)\mathbf{I}&\frac{S_0(2\psi)}{2}\\ \frac{R_0(2\psi)}{2}\mathbf{I}&-S_0(2\psi)\mathbf{I}&-\frac{R_0(2\psi)}{2}\end{bmatrix}. \tag{69}$$

Now, the coefficients $\mathbf{h}_1(\vartheta)$, $\mathbf{h}_2(\vartheta)$ and $\mathbf{h}_3(\vartheta)$ can be given according to Eqn. (63), therefore the second order approximation (59) of the center manifold is available. Using Eqns. (56) and (59), we obtain a third-order approximation in terms of z_1 and z_2 of the nonlinear part in the first two rows of Eqn. (58). This way we get the critical subsystem in the normal form

$$\begin{bmatrix}z_1'\\ z_2'\end{bmatrix}=\begin{bmatrix}0&\omega\\ -\omega&0\end{bmatrix}\begin{bmatrix}z_1\\ z_2\end{bmatrix}+\begin{bmatrix}\sum_{j+k=2,3}a_{jk}z_1^jz_2^k\\ \sum_{j+k=2,3}b_{jk}z_1^jz_2^k\end{bmatrix}. \tag{70}$$

Thereafter, the analysis of the Hopf bifurcation and the calculation of periodic orbits can be performed on the two-dimensional system (70) instead of the infinite-dimensional one (37).

3 ESTIMATION OF THE UNSAFE ZONE

First we analyze the criticality of the Hopf bifurcation, which can be determined based on the sign of the Poincaré-Lyapunov constant (PLC). The bifurcation is subcritical when the PLC is positive and supercritical when it is negative. [22] provides the following formula for the PLC:

$$\Delta=\frac{1}{8\omega}[(a_{20}+a_{02})(-a_{11}+b_{20}-b_{02}) \\ +(b_{20}+b_{02})(b_{11}+a_{20}-a_{02})] \\ +\frac{1}{8}(3a_{30}+a_{12}+b_{21}+3b_{03}). \tag{71}$$

In our case, this formula gives

$$\Delta=\frac{(1-\cos\psi)p\gamma}{2}(3\eta_3-\delta\eta_2^2). \tag{72}$$

The coefficient δ contains a complicated ψ-dependent expression, namely

$$\delta=1-\frac{S_0q_1-R_0q_2}{-R_0q_1-S_0q_2}\frac{2p_{\mathrm{st}}\left(4\zeta\omega R_{02}+(4\omega^2-1)S_{02}\right)}{[p_{\mathrm{st}}R_{02}-(4\omega^2-1)]^2+[p_{\mathrm{st}}S_{02}+4\zeta\omega]^2} \\ +\frac{p_{\mathrm{st}}^2(R_{02}^2+S_{02}^2)-(4\omega^2-1)^2-(4\zeta\omega)^2}{[p_{\mathrm{st}}R_{02}-(4\omega^2-1)]^2+[p_{\mathrm{st}}S_{02}+4\zeta\omega]^2}, \tag{73}$$

where $R_{02}(\psi)=R_0(2\psi)$ and $S_{02}(\psi)=S_0(2\psi)$. The PLC was numerically determined for several case studies, and it was found to be positive for realistic cutting-force distributions, which indicates the subcritical nature of machining processes. In the special case of concentrated cutting-force with $w(\theta)=\delta(\theta)$, the subcriticality of the Hopf bifurcation was proved in [17]. Here, we do not prove the subcriticality for general $w(\theta)$ kernel, as the expression of the PLC is too complicated. However, the function $\Delta(\psi)$ was plotted for each case study under investigation, and no supercritical case was encountered.

The subcritical Hopf bifurcation gives rise to an unstable periodic orbit around the linearly stable equilibrium, which has a finite domain of attraction. Therefore, once a perturbation (e.g. material inhomogeneity) moves the system out of the domain of attraction, the amplitude of the arising vibrations will grow, large-amplitude chatter will evolve, and the system will not settle down to the steady state. However, the amplitude of the vibrations cannot take arbitrarily large values, since at certain amplitudes the tool leaves of the workpiece and loses contact. Then the tool undergoes a damped free oscillation until it gets back to the workpiece again. This effect stabilizes the system in the sense that it limits the chatter amplitude to a finite value. As shown by the subcriticality of the Hopf bifurcation, for certain parameter regions linearly stable cutting and large-amplitude chatter may coexist. This domain is referred to as region of bistability or unsafe zone. In this domain, although the system is linearly stable, a perturbation may push the system outside of the domain

of attraction of the linearly stable stationary cutting, and large amplitude vibrations (chatter) may occur.

The width of the bistable region is determined by the basin of attraction of stationary cutting. According to [23], the amplitude of the resulting limit cycle can be calculated approximately as

$$r(\psi,p)\approx\sqrt{-\frac{\gamma(\psi)}{\Delta(\psi)}(p-p_{\mathrm{st}}(\psi))}\,. \tag{74}$$

It is important to emphasize the difference between the actual bifurcation parameter value p and the stability limit $p_{\mathrm{st}}(\psi)$. The approximate periodic orbit of amplitude $r(\psi,p)$ assumes the form

$$\mathbf{y}_t(\vartheta)\approx r(\psi,p)\left[\cos(\omega t)\mathbf{s}_{\mathrm{R}}(\vartheta)-\sin(\omega t)\mathbf{s}_{\mathrm{I}}(\vartheta)\right]\,, \tag{75}$$

which yields the solution

$$\mathbf{y}(t)\approx r(\psi,p)\left[\cos(\omega t)\mathbf{s}_{\mathrm{R}}(0)-\sin(\omega t)\mathbf{s}_{\mathrm{I}}(0)\right]\,. \tag{76}$$

The corresponding tool position is

$$\xi(t)=y_1(t)\approx r(\psi,p)\cos(\omega t)\,. \tag{77}$$

The unstable limit cycle exists only in the case where the tool does not lose contact with the workpiece during the periodic oscillation and Eqn. (22) governs the tool motion. Once loss of contact occurs, the unstable periodic orbit vanishes. Consequently, the region of bistability is limited by the so-called switching line where the tool loses contact with the workpiece due to the large-amplitude vibrations. At loss of contact the chip thickness $h(t,\theta)$ drops to zero, hence the dimensionless form of Eqn. (13) yields the switching condition

$$1+\xi(t-\tau+\theta)-\xi(t+\theta)=0\,. \tag{78}$$

We can reformulate the switching condition by substituting the periodic solution (77)

$$\begin{aligned}1=&\xi(t+\theta)-\xi(t-\tau+\theta)\\ =&r(\psi,p)\left[\cos(\omega(t+\theta))-\cos(\omega(t-\tau+\theta))\right]\\ =&r(\psi,p)\sqrt{(1-\cos\psi)^2+\sin^2\psi}\cos\left(\omega(t+\theta)+\phi\right)\,,\end{aligned} \tag{79}$$

where ϕ is a phase shift. If there exists any pair of t and θ such that the switching condition is fulfilled, then loss of contact happens and the periodic orbit disappears. In order to find the smallest amplitude for which $h(t,\theta)=0$ occurs, we write $\cos\left(\omega(t+\theta)+\phi\right)=1$. Substituting the approximate amplitude (74) and rearranging Eqn. (79) for p, we get the bistable limit in the form

$$p_{\mathrm{bist}}(\psi)=-\frac{\Delta(\psi)}{\gamma(\psi)}\cdot\frac{1}{2}\cdot\frac{1}{1-\cos\psi}+p_{\mathrm{st}}(\psi)\,. \tag{80}$$

Fig. 4 shows a series of stability charts with the linearly stable and bistable limits of the system assuming $\zeta=0.02$, $\varepsilon=0.05$, and $\alpha=0.4$. The presented stability boundaries are all calculated analytically. It is known for concentrated cutting-force model that the minima of the linear stability lobes lie on a $p=$ const line (see e.g. [26]). However, as shown in Fig. 4, it is not the case for distributed cutting-force model as the stability lobes shift upwards in case of low spindle speeds. Furthermore, we can see that the bistable region grows with the linearly stable region. Therefore, the ratio of the width of the bistable region and the width of the linearly stable region will be investigated. We can express the relative width $\Delta p(\psi)$ of the bistable region in the form

$$\Delta p(\psi)=\frac{p_{\mathrm{st}}(\psi)-p_{\mathrm{bist}}(\psi)}{p_{\mathrm{st}}(\psi)}=\frac{1}{4}\left(3\eta_3-\delta(\psi)\eta_2^2\right). \tag{81}$$

Numerical case studies for the plateau-and-decay kernel (9) show that the magnitude of $|\delta(\psi)|$ is quite small, around $10^{-5}..10^{-2}$. It was found to be true for the usual small values of the parameters ζ and ε, irrespective of the kernel shape given by α (we investigated parameter ranges $\zeta=0.001..0.2$, $\varepsilon=0.001..0.2$, $\alpha=0..1$). Since the coefficients η_2^2 and η_3 are usually in the same order of magnitude, the term $\delta(\psi)\eta_2^2$ is negligible compared to $3\eta_3$, and we get a very simple estimate for the width of the bistable region:

$$\Delta p_{\mathrm{est}}=\frac{3}{4}\eta_3\,. \tag{82}$$

Note that after omitting $\delta(\psi)$ we get the same unsafe zone width irrespective of both the spindle speed Ω and the shape $w(\theta)$ of the cutting-force distribution. Consequently, the same estimate works for concentrated cutting-force models as well, which was also shown in [17]. In the case of the Taylor-force ($\eta_3=5/96$) the formula gives $\Delta p_{\mathrm{est}}=0.039$. It is in good agreement with [17, 25], where the width of the unsafe zone was shown to be 4% at the notches of the lobes for concentrated cutting-force. In the case of the Tobias-force the size of the bistable region depends on the mean chip thickness h_0 as shown in Fig. 5. For small h_0, Δp_{est} first increases with h_0, then peaks at a critical mean chip thickness, and in the end it tends to a constant 25%

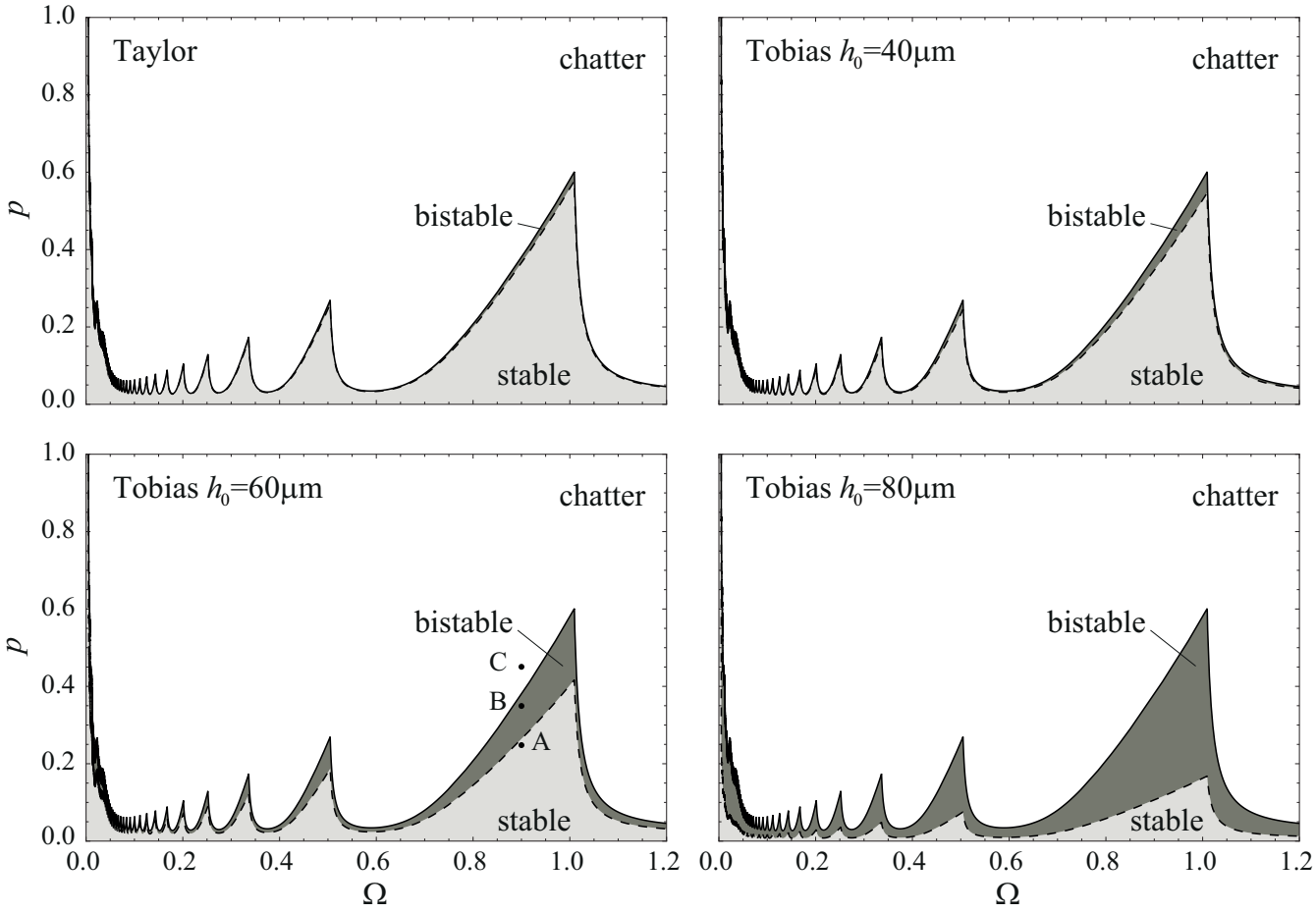

FIGURE 4. ANALYTIC STABILITY CHARTS OF THE NONLINEAR TURNING MODEL WITH FORCE DISTRIBUTION (9).

value. According to [17], the critical mean chip thickness is $h_{\mathrm{cr}} = -\rho_1/\rho_2 = 113\ \mu$m. Around h_{cr} the width of the unsafe zone exceeds 100%. This shows that the analytic results on the bistable limit lose accuracy at this point, since formula (74) for the amplitude of periodic orbits is valid only in the vicinity of the linear stability boundaries. Therefore, the analytic results can only be trusted for small and very large mean chip thickness values, where the unsafe zone is not too wide.

Finally, the solution of Eqn. (22) is presented in Fig. 6 for four different cases. The solutions were obtained numerically via approximating the distributed delay term in Eqn. (22) by a sum of 20 point delays and using the solver dde23 in Matlab. Panels A, B1, B2, and C correspond to points A, B, and C in the bottom left corner of Fig. 4. The corresponding dimensionless spindle speed is $\Omega = 0.9$, whereas the dimensionless chip width values are $p =$ 0.25, 0.35, and 0.45, respectively. All other parameters were kept the same as in the bottom left panel of Fig. 4. The initial state used in the numerical simulations was a constant function: $\xi(t) \equiv \xi_{\mathrm{init}}$, $t < 0$. As point A in Fig. 4 is in the globally stable region, panel A of Fig. 6 shows an asymptotically stable solution for $\xi_{\mathrm{init}} = 1$. As for point B, it lies in the bistable parameter region of the stability chart. In this case, as Fig. 6 demonstrates, stable and unstable solutions can also occur depending on the initial conditions: panel B1 shows a stable solution for $\xi_{\mathrm{init}} = 0.5$, and panel B2 presents an unstable one for $\xi_{\mathrm{init}} = 1$. Point C in Fig. 4 is part of the unstable region, thus for $\xi_{\mathrm{init}} = 0.5$ the solution in panel C of Fig. 6 is unstable.

CONCLUSIONS

We can conclude that the cutting-force distribution along the tool's rake face has an important effect on the stability of the machining process. Namely, it enhances the stability at small spindle speeds and allows chatter-free operation with larger depth of cut values, by which the material removal rate of low-speed cutting processes can be increased. Besides, the widening of the stable region at low spindle speeds can be enhanced by maintaining larger contact surface between the tool and the chip (achieving

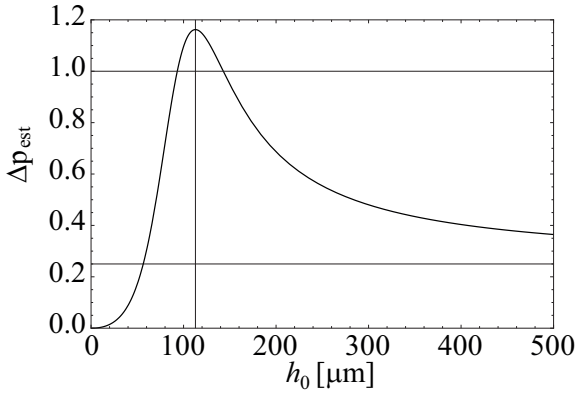

FIGURE 5. ESTIMATE OF THE RELATIVE WIDTH OF THE UNSAFE ZONE ASSUMING TOBIAS-FORCE.

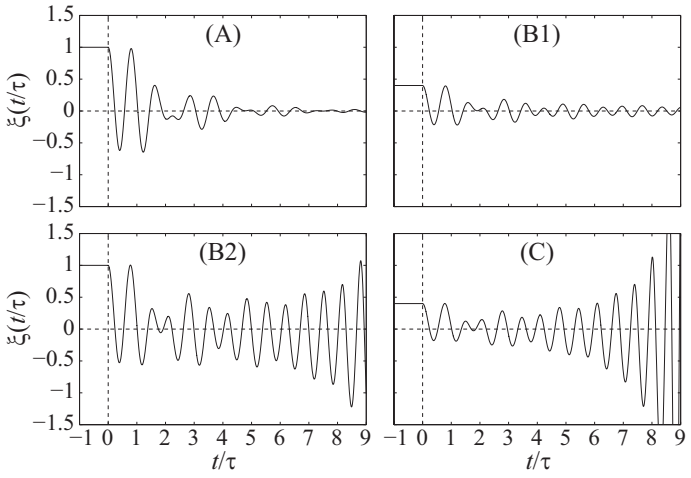

FIGURE 6. NUMERICAL SOLUTIONS OF EQN. (22) CORRESPONDING TO POINTS IN THE STABLE (A), BISTABLE (B1, B2), AND UNSTABLE (C) PARAMETER REGIONS.

larger ε values). This phenomenon is caused by the short regenerative effect, which alters the stability limits also at high spindle speeds in some cases (see [10]). The short regenerative effect is represented by an additional short distributed delay in the governing equations of the system. The added delay accounts for the seemingly unimportant fact that the chip needs a certain amount of time to slip along the tool's rake face. As such a small effect makes qualitative changes in the system behavior, we can conclude that multiscale phenomena hide behind the dynamics of machining processes.

The subcritical nature of orthogonal cutting processes was shown for realistic cutting-force distributions. Accordingly, there exists an unsafe zone near the stability limits, where linearly stable cutting and large-amplitude chatter coexist. If the cutting-force characteristic has no inflection, then the unsafe zone is thin, it occupies only around 4% of the linearly stable region. However, when the cutting-force characteristic possesses an inflection point, then the bistable region is significantly wider. Nevertheless, as the bistable limits seem to follow the linear stability boundaries, it is still reasonable to operate the system in one of the peaks of the linear stability chart. Besides, in case of a cutting-force characteristic with an inflection point, the width of the unsafe zone depends on the mean chip thickness and peaks for a critical feed per revolution value. Therefore, this feed per revolution range should be avoided, which can be done even by increasing the mean chip thickness and the productivity.

Note that here we used third-order expansion of the nonlinear terms, which gives a second-order approximation of the amplitude of the limit cycle as a function of the bifurcation parameter p. More accurate approximation can be obtained by higher-order expansion, however, the criticality of the bifurcation is already determined by the third-order approximation.

ACKNOWLEDGMENT

This work was supported by the Hungarian National Science Foundation under grant OTKA-K105433. The research leading to these results has received funding from the European Research Council under the European Unions Seventh Framework Programme (FP/2007-2013) / ERC Advanced Grant Agreement n. 340889.

REFERENCES

[1] Tobias, S. A., and Fishwick, W., 1958. "Theory of regenerative machine tool chatter". *The Engineer*, Feb., pp. 199–203, 238–239.

[2] Tlusty, J., and Polacek, M., 1963. "The stability of the machine tool against self-excited vibration in machining". In ASME Production Engineering Research Conference, pp. 454–465.

[3] Burns, T. J., and Davies, M. A., 1997. "Nonlinear dynamics model for chip segmentation in machining". *Physical Review Letters,* ***79***(3), pp. 447–450.

[4] Burns, T. J., and Davies, M. A., 2002. "On repeated adiabatic shear band formation during high-speed machining". *International Journal of Plasticity,* ***18***, pp. 487–506.

[5] Pálmai, Z., and Csernák, G., 2009. "Chip formation as an oscillator during the turning process". *Journal of Sound and Vibration,* ***326***, pp. 809–820.

[6] Stepan, G., 1989. *Retarded dynamical systems*. Longman, Harlow.

[7] Clancy, B. E., and Shin, Y. C., 2002. "A comprehensive chatter prediction model for face turning operation including tool wear effect". *International Journal of Machine Tools and Manufacture,* ***42***(9), pp. 1035–1044.

[8] Ahmadi, K., and Ismail, F., 2010. "Experimental investigation of process damping nonlinearity in machining chatter". *International Journal of Machine Tools and Manufacture,* ***50***(11), pp. 1006–1014.

[9] Shi, Y., Mahr, F., von Wagner, U., and Uhlmann, E., 2012. "Chatter frequencies of micromilling processes: Influencing factors and online detection via piezoactuators". *International Journal of Machine Tools and Manufacture,* ***56***, pp. 10–16.

[10] Stepan, G., 1998. "Delay-differential equation models for machine tool chatter". In *Nonlinear Dynamics of Material Processing and Manufacturing*, F. C. Moon, ed. John Wiley and Sons, New York, pp. 165–192.

[11] Barrow, G., Graham, W., Kurimoto, T., and Leong, Y. F., 1982. "Determination of rake face stress distribution in orthogonal machining". *International Journal of Machine Tool Design and Research,* ***22***(1), pp. 75–85.

[12] Buryta, D., Sowerby, R., and Yellowley, I., 1994. "Stress distributions on the rake face during orthogonal machining". *International Journal of Machine Tools and Manufacture,* ***34***(5), pp. 721–739.

[13] Bagchi, A., and Wright, P. K., 1987. "Stress analysis in machining with the use of sapphire tools". *Proceedings of the Royal Society of London, Series A, Mathematical and Physical Sciences,* ***409***(1836), pp. 99–113.

[14] Stepan, G., Dombovari, Z., and Munoa, J., 2011. "Identification of cutting force characteristics based on chatter experiments". *CIRP Annals - Manufacturing Technology,* ***60***(1), pp. 113–116.

[15] Taylor, F. W., 1907. *On the art of cutting metals*. American Society of Mechanical Engineers, New York.

[16] Shi, H. M., and Tobias, S. A., 1984. "Theory of finite amplitude machine tool instability". *International Journal of Machine Tool Design and Research,* ***24***(1), pp. 45–69.

[17] Dombovari, Z., Wilson, R. E., and Stepan, G., 2008. "Estimates of the bistable region in metal cutting". *Proceedings of the Royal Society A - Mathematical, Physical and Engineering Sciences,* ***464***, Aug., pp. 3255–3271.

[18] Zorev, N. N., 1963. "Inter-relationship between shear processes occurring along tool face and shear plane in metal cutting". *ASME International Research in Production Engineering*, pp. 42–49.

[19] Chandrasekaran, H., and Thuvander, A., 1998. "Modeling tool stresses and temperature evaluation in turning using finite element method". *Machining Science and Technology,* ***2***(2), pp. 355–367.

[20] Altintas, Y., 2000. *Manufacturing Automation - Metal Cutting Mechanics, Machine Tool Vibrations and CNC Design*. Cambridge University Press, Cambridge.

[21] Atkins, T., 2014. "Prediction of sticking and sliding lengths on the rake faces of tools using cutting forces". *International Journal of Mechanical Sciences*, p. In Press.

[22] Hassard, B. D., Kazarinoff, N. D., and Wan, Y.-H., 1981. *Theory and Applications of Hopf Bifurcation*. London Mathematical Society Lecture Note Series **41**, Cambridge.

[23] Guckenheimer, J., and Holmes, P., 1983. *Nonlinear Oscillations, Dynamical Systems, and Bifurcations of Vector Fields*. Springer, New York.

[24] Hale, J., 1977. *Theory of Functional Differential Equations*. Springer, New York.

[25] Stepan, G., and Kalmar-Nagy, T., 1997. "Nonlinear regenerative machine tool vibrations". In Proceedings of DETC'97, ASME Design and Technical Conferences, pp. 1–11.

[26] Insperger, T., and Stepan, G., 2011. *Semi-Discretization for Time-Delay Systems - Stability and Engineering Applications*. Springer, New York.